IEEE Access
Multidisciplinary | Rapid Review | Open Access Journal

SPECIAL SECTION ON MISSION CRITICAL SENSORS AND SENSOR NETWORKS (MC-SSN)

Received August 14, 2019, accepted August 22, 2019, date of publication September 10, 2019,
date of current version September 25, 2019.

Digital Object Identifier 10.1109/ACCESS.2019.2940561

Study on Weather Radar Echo Data Generation Based on DCGAN

HAIJIANG WANG[1], MENGQING GAO[1], SHIPENG HU[1], ZHAOPING SUN[2], AND ZILI XU[3]

[1]College of Electronic Engineering, Chengdu University of Information Technology, Chengdu 610225, China
[2]Beijing Metstar Radar Company Ltd., Beijing 100096, China
[3]Second Research Institute of CAAC, Chengdu 610041, China

Corresponding author: Haijiang Wang (whj@cuit.edu.cn)

This work was supported by the National Natural Science Foundation of China under Grant U1733103.

ABSTRACT Doppler weather radar can detect the changes in precipitation clouds for short-term forecasting. In the process of development of Doppler weather radar and weather identification algorithms, some typical Doppler weather radar base data corresponding to different weather phenomena are necessary for signal processing unit test and algorithm verification. However, the existing real weather radar base data with high quality can't meet the requirement in amount. In this paper, an algorithm based on Deep Convolutional Generative Adversarial Networks (DCGAN) to generate typical weather radar base data is proposed. And in the test signal simulation step, the power spectrum algorithm is improved. The results show that the data produced by the DCGAN have the same characteristics with the real weather radar base data without obvious non-meteorological noise. Moreover, the improved power spectrum algorithm performs better in terms of accuracy rate of the simulation echo signal.

INDEX TERMS Doppler weather radar base data simulation, baseband weather radar echo signal, DCGAN, power spectrum simulation.

I. INTRODUCTION

Doppler weather radar detects meteorological targets by transmitting microwave that can penetrate cloud and rain. Radar pulse propagates out by radar transmitter, then the pulse is scattered by a hydrometeor and returns to the receiver where it is transformed from a microwave pulse to one that can be displayed on video equipment. Doppler weather radar is extensively applied as an important remote sensor for the sounding and short-term forecasting of hazardous weather [1]. So the development of high-performance Doppler weather radar and robust weather phenomena identification algorithms are two significant issues.

In the stage of development of Doppler weather radar, some echo signals corresponding to different weather phenomena are required as test signals to evaluate the performance of the signal processing unit. But the desired echo signals are not always available for application owing to the lack of observable weather events or applicable radar instruments. Thus, echo signal simulation with existing weather radar base data is an alternative we can turn to. Furthermore, in the research process of weather identification based on weather radar base data, large amounts of typical weather radar base data are needed for the algorithm verification. The applications of weather radar base data are shown in Figure 1.

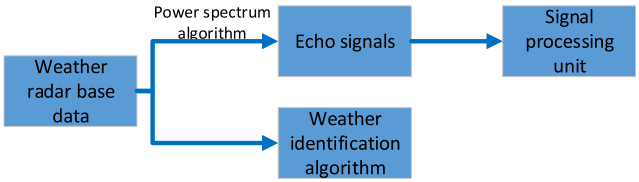

FIGURE 1. The applications of weather radar base data.

However, the accessible real weather radar base data are much less than needed for the development of Doppler weather radar and weather identification algorithms. Hence typical weather radar base data simulation is a way we must choose to produce the required amount of data. Several researchers explored the simulation of weather radar base data and echo signals. Zrnic proposed a power spectrum simulation algorithm to generate weatherlike Doppler spectra and signals for determining radar systems' behavior under adverse conditions [2]–[4]. Bousquet *et al.* established a small-scale wind field model [5], the wind field is related to real landform,which needs a huge amount of data

The associate editor coordinating the review of this manuscript and approving it for publication was Qilian Liang.

storage space. Lischi *et al.* adopted the Weather Research and Forecast (WRF) model combined the Transmission Matrix code (T-Matrix) to simulate radar echo signals [6], [7]. This method takes multiple rainfall parameters as input and has the shortcoming of high dependence on real weather radar base data. Zhengang *et al.* designed a mathematical model to simulate the weather radar base data which can reflect typical weather phenomena [8]. However, this model only implies part of characteristics of real data. The Generative Adversarial Networks (GAN) is a Deep Learning algorithm [9] proposed by Goodfellow, which has been widely applied in image processing and artificial image generation. The generated images by GAN can imitate the features of real ones well. For example, some generated handwritten digits and human faces can pass fake imitation for genuine [10]. Many researchers have carried out GAN-based experiments and showed the advantages of GAN in various applications. Wenqi *et al.* utilized GAN to synthesize human images from masks [10]. Zhang *et al.* proposed a star-galaxy image generation method based on GAN [11] to generate star-galaxy images with two different resolutions. Isola *et al.* implemented image style transfer in different scenarios by using GAN [12]. Yuanzhao *et al.* used GAN to predict the precipitation [13] and showed that GAN could recognize the characteristics of radar echo image.

Deep Convolutional Generative Adversarial Networks (DCGAN) is an improvement of GAN [14], where the convolutional neural network (CNN) is applied to extract the features from the original data. CNN can improve the stability of DCGAN and shorten the training time [15], [16]. As a special data, weather radar base data are color coded. The color coded data can be visualized on a plan position indicator (PPI). The PPI images are used as the input of DCGAN to simulate weather radar base data. The simulated weather radar base data have the same characteristics with the real ones. Furthermore, with DCGAN, a dataset including reflectivity, velocity and spectral width can be generated simultaneously. So the deficiency problem of weather radar data can be solved by DCGAN simulation. With the generated weather radar base data from DCGAN, the baseband weather radar echo signals can be obtained by using the improved power spectrum algorithm.

This paper is organized as follows: Section II describes the datasets for the DCGAN training. Section III presents the weather radar base data generation method and the radar echo signals simulation method. Section IV evaluates the simulation results. Section V discusses the advantages and disadvantages of these methods. Section VI concludes this study.

II. DATA

In this research, a rich data set has been constructed, which includes 2000 samples. It is selected from a large amount of radar base data detected by multiple CINRAD_SA single-polarized radars during 2002-2008. Each radar base data contains three parts which are the reflectivity data, the velocity data and the spectral width data. The main parameters of the radar base data format are shown in Table 1.

TABLE 1. The main parameters of the weather radar base data format.

Number	Parameter	Value
1	Range Bin Number of Reflectivity	200
2	Range Bin Number of Velocity	800
3	Range Bin Number of Spectral Width	800
4	Range Bin Length of Reflectivity	1000 m
5	Range Bin Length of Velocity	250 m
6	Range Bin Length of Spectral Width	250m
7	Elevation	2.4°
8	Wave width	1°
9	Radial Number	360（formatted）

In meteorological services, the CINRAD-SA radar mostly adopts the volume scan mode to obtain the three-dimensional distribution of precipitation clouds in atmosphere. The radar completes 360-degree scanning with a fixed elevation, and then changes the elevation to enter the next layer scanning. The spatial resolution increases with the raise of elevation and slope distance, which means it is difficult to apply the radar base data directly to the DCGAN model. Before using the radar base data to train the DCGAN model, it is necessary to preprocess the radar base data, including the standardization and the PPI mapping. The standardization can be summarized as

$$\begin{cases} \bar{X} = \dfrac{X - X_{Min}}{X_{Max} - X_{Min}} \times 255 \\ \bar{X} = 0 \quad (X \ is \ \text{Null}) \end{cases} \tag{1}$$

where, X is the input to the normalized function, and $\bar{X}$ is the output after standardization. Moreover, X_{Max} and X_{Min} correspond to the maximum and minimum values of radar base data respectively, which are listed in Table 2. As shown in Table 1, the range bin length of reflectivity is different from that of velocity and spectral width. In order to maintain consistency between multiple product data, each range bin of reflectivity is duplicated four times to form a new matrix.

TABLE 2. The data formats after preprocessing.

Object	Matrix size	Rang of valid values	Maximum value	Minimum value
Z	360*800	-15-75dBz	75dBz	-25dBz
V	360*800	-25-25m/s	25m/s	-30m/s
W	360*800	0-10m/s	10m/s	-5m/s

The gray colormap is applied to draw the PPI image of radar base data, including the reflectivity (Z), velocity (V) and spectral width (W). Moreover, each PPI image with a size of 400*800. As shown in Figure 2, three PPI images are used

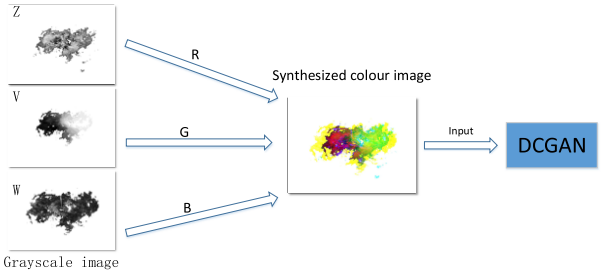

FIGURE 2. The PPI images preprocessing.

for the input of DCGAN, which can be regarded as the three channels data of RGB image.

Finally, the output of the DCGAN is a three-channel color image corresponding to the reflectivity, velocity and spectral width data respectively. Moreover, the radar Radial data can be obtained by sampling the color image in the radial direction.

III. METHOD

A. WEATHER RADAR BASE DATA GENERATION

1) THE PRINCIPLE OF DCGAN

The DCGAN consists of two parts: the generating network (generator, G) and the discriminating network (discriminator, D). The DCGAN value function can be seen as a game learning model about the generating network and the discriminating network. In generating network, the input is a random noise or a latent variable. The discriminator can be regarded as a binary classifier to discriminate whether the input data are real or artificial. The generator and discriminator improve their imitation and discriminant abilities respectively through the game learning process. The model of DCGAN is shown in Figure 3.

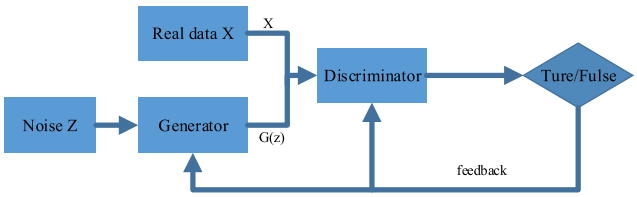

FIGURE 3. The model of DCGAN.

2) THE STRUCTURE OF GENERATOR NETWORK

The architecture of the generating network is shown in Figure 4, in which the input is a 100-dimensional random noise vector. The fractional-strided convolution is applied to repalce the pooling layers in the generating network, which can increase the input size. Moreover, the Batch Normalization is applied to normalize the input to each unit to have zero mean and unit variance. In addition, the fully connected hidden layers are removed for deeper architectures. Then the generator uses Rectified Linear Units (ReLU) activation for all layers except for the output which uses the hyperbolic

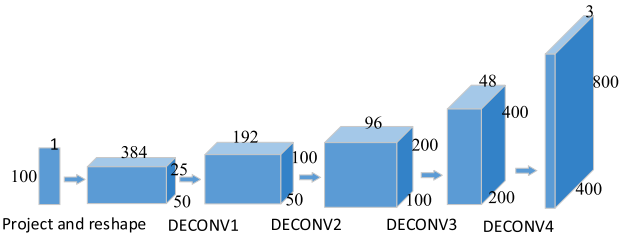

FIGURE 4. The architecture of generator.

tangent (Tanh) activation. The Tanh is a zero-mean function which can improve training efficiency. ReLU and Tanh are determined by equation (2) and equation (3), respectively.

$$.\mathrm{Re}\,LU(x) = \begin{cases} x, & x > 0 \\ 0, & x \le 0 \end{cases} \tag{2}$$

$$Tanh(x) = \frac{e^{x} - e^{-x}}{e^{x} + e^{-x}} \tag{3}$$

3) THE STRUCTURE OF DISCRIMINATOR NETWORK

As shown in Figure 5, the architecture of discriminator can identify the generated data and the real data. The discriminator of DCGAN is different from the traditional GAN proposed by Ian Goodfellow [9]. The discriminator replaces all pooling layers with strided convolutions. It uses Batch Normalization to resolve the problem that the poor initialization and the gradient flow in deeper models. The discriminator uses LeakyReLU activation in all layers.

$$Leaky\ \mathrm{Re}\,LU(x) = \begin{cases} x & x > 0 \\ 0.2x & x \le 0 \end{cases} \tag{4}$$

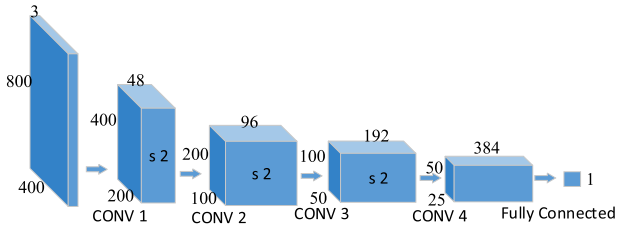

FIGURE 5. The architecture of discriminator.

When the gradient is less than 0, the neurons can be activated, so that it can improve the stability of the training. The final fully connected layer has only one output node, and the output value of the network is mapped to probability by using the sigmoid function.

$$simgoid(x) = \frac{1}{1 + e^{-x}} \tag{5}$$

4) THE TRAINING PROCESS OF DCGAN

The steps of DCGAN implementation are as follows:

The first step is to calculate the loss function $V(G)$:

$$V(G) = (1 - y)\log(1 - D(G(z))) \tag{6}$$

where, y is the parameter for balancing losses. In this paper, z is a 100-dimensional random noise vector, $G(z)$ is the output of generator, and $D(G(z))$ represents the true probability of the data generated by the G.

The second step is to calculate the loss function $V(D)$:

$$V(D) = -((1-y)\log(1-D((G(z))) + y\log D(x)) \quad (7)$$

where, x is the real sample data, and $D(x)$ represents the true probability of the real sample data.

The third step is to calculate the optimization function, and the mathematics model is expressed as:

$$\min_G \max_D V(D,G) = E_{x\sim P_{data}(x)}(\log D(x)) + E_{z\sim P_z}(\log(1-D(G(z)))) \quad (8)$$

In which P_{data} is the distribution of real data, and P_z is the distribution of random noise. When the discriminator's input x comes from data, the output is close to 1. When the discriminator's input z comes from noise variables, the output is close to 0. The stronger the ability of D is, the bigger $D(x)$ and the smaller $D(G(z))$ will be so that $V(D, G)$ will become larger. It is a time to finish the training when the generated data are very close to the real data and D cannot judge.

B. BASEBAND RADAR ECHO SIGNAL SIMULATION

1) PRINCIPLE OF POWER SPECTRUM ALGORITHM

The method of I/Q time-domain sequence simulated by the traditional power spectrum algorithm which can be abbreviated PS is proposed by Zrnic [2], [3]. The I/Q time-domain sequence is the radar echo signal. Zrnic proposed that the power spectrum distribution of weather echo signal is very similar to the Gaussian distribution. The power spectrum function [2] can be defined as:

$$P_n(f_k) = \frac{p_r}{\sqrt{2\pi}\delta_f}\exp[-\frac{(f_k-f_d)^2}{2\delta_f^2}]\cdot\frac{1}{p_0} \quad (9)$$

Here $f_d = 2v_r/\lambda$ is the Doppler frequency, v_r is the radial velocity, $\delta_f = 2\delta_v/\lambda$ is the standard deviation of f_d, δ_v is the spectrum width, and p_0 is the mean value of multiple Gauss power spectral components and is defined in equation (10). It guarantees that the signal power keeps constant when defining the power spectrum function.

$$p_0 = \frac{1}{N}\sum_{k=0}^{N-1}\frac{1}{\sqrt{2\pi}\delta_f}\exp[-\frac{(f_k-f_d)^2}{2\delta_f^2}] \quad (10)$$

and frequency f_k is

$$f_k = -PRF/2 + k\cdot PRF/N (k = 0, 1, 2\cdots N-1) \quad (11)$$

Here, PRF is pulse repetition frequency, N is the number of sampling sites. $p_r = CZ/r^2$ is echo power where Z is radar reflectivity, r is radial distance between meteorology object and radar, and C is radar constant that depends on radar parameters [17], which is defined as:

$$C = 0.93\frac{\pi^3}{1024\ln 2}\frac{P_t G^2 h\theta\varphi}{\lambda^2} \quad (12)$$

where, P_t is transmitting power, G is antenna gain, θ is horizontal beamwidth, φ is vertical beamwidth, λ is the wavelength of the electromagnetic wave emitted by the radar, and h is pulse length.

In general, the true signal power spectrum is mixed with noise. In order to simulate the true power spectrum characteristics of weather signal, it is necessary to add noise in equation (9) and then randomize it [2]. Adding noise power spectrum P_N/PRF to equation (9) and multiplying this new equation by $-\ln(1-rnd)$ to get a randomized function, the result is shown in equation (13).

$$P_n(f_k) = -\ln(1-rnd)\{\frac{p_r}{\sqrt{2\pi}\delta_f}\exp[\frac{-(f_k-f_d)^2}{2\delta_f^2}]\cdot\frac{1}{p_0} + P_N/PRF\} \quad (13)$$

where, P_N is noise power, and rnd is a random variance uniformly distributed between 0 and 1. The Inverse Discrete Fourier Transform (IDFT) is used to obtain the time-domain sequences [2] $s(i)$:

$$s(i) = I(i) + jQ(i) = \frac{1}{N}\sum_{k=1}^{N}(\sqrt{P_n(f_k)}\exp(j\theta_k)\exp(-j\frac{2\pi}{N}ki) \quad (14)$$

where, θ_k is a uniformly distributed phase between 0 and 2π; and $P_n(f_k)$ and θ_k are statistically independent.

2) POWER SPECTRUM ALGORITHM WITH ADAPTIVE SPECTRUM SCOPE

The traditional power spectrum algorithm is used to simulate weather radar test signals. The quality of partial areas of these simulated signals is poor. When analyzing the data in these areas separately, it is found that the deviation of simulated signal is large when the radial velocity is too large or too small. When using traditional algorithms to calculate the echo power spectrum, a problem is that it will make part of power spectrum components beyond the spectrum scope when the velocity is too large or too small. In order to solve this problem, a power spectrum algorithm with adaptive spectrum scope (which can be called adaptive power spectrum algorithm and can be abbreviated APS) is applied in this paper. In this algorithm, the spectrum scope is selected according to the velocity automatically. Suppose $PRF = 1000Hz$, the frequency f_k corresponding to different velocity is defined in equation (15).

$$f_k = \begin{cases} -k\cdot PRF/N, & v_r < -12 \\ -PRF/2 + k\cdot PRF/N, & -12 < v_r < 12 \\ k\cdot PRF/N, & v_r > 12 \end{cases} \quad (15)$$

Assume that the value of reflectivity is 30 dBz, velocity is 20 m/s, and spectral width is 3 m/s. Based on these assumptions, the power spectrum is shown in Figure 6. Figure 6(a) shows the power spectrum using PS, and Figure 6(b) shows the power spectrum using APS in the same condition. The PS discards a portion of the power spectrum components because

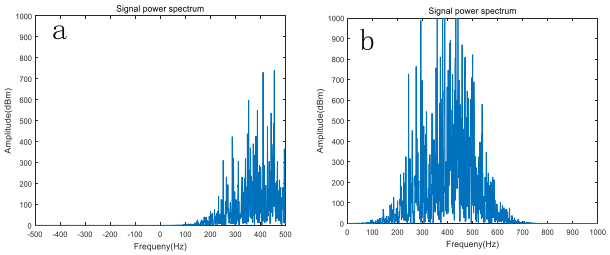

FIGURE 6. The power spectrum calculated by PS (a) and APS (b).

of the spectrum scope limitations, while the power spectrum components are almost completely retained when using APS to adjust the spectrum scope.

When the radar parameters are known, echo signals with real weather object characteristics can be simulated based on weather radar base data. Weather radar base data can be calculated by I/Q time-domain sequences and the calculation can be used as a module to verify the accuracy of the simulation algorithm. At present, the weather radar signal processor mainly uses Pulse Pair Processing (PPP) algorithm and the Fast Fourier Transform (FFT) algorithm [18], [19]. The estimation accuracy of FFT algorithm is higher, therefore the FFT algorithm is adopted in this paper.

IV. EXPERIMENT ANALYSIS

A. ANALYSIS OF REAL WEATHER RADAR ECHO IMAGES

The base data of Doppler weather radar contains information about reflectivity, velocity and spectral width. The reflectivity is related to liquid water content or precipitation rate in the resolution volume and it can be calculated by the weather signal power. Previous studies have shown that precipitation is likely to occur where reflectivity is greater than 10 dBz [20]. And the higher the reflectivity is, the stronger the precipitation intensity is. As shown in Figure 7, the precipitation intensity in the marked areas is much stronger than that in the surrounding areas. Besides, the reflectivity has been decreased from the center to the edge, and the edge is uneven. Based on Doppler effects, Doppler weather radar can measure the relative velocity of precipitation particles to the beam emitted by radar. Relative velocity means that velocity vectors exist both toward and away from the radar. Therefore, there is both positive and negative velocity in the PPI image of velocity as shown in Figure 7. The spectral width is a measure of the velocity dispersion, that is, shear or turbulence within the resolution volume. Most of the spectral width is less than 2m/s. The reflectivity and velocity are positively related with spectral width, which is consistent with known experience [21], [22].

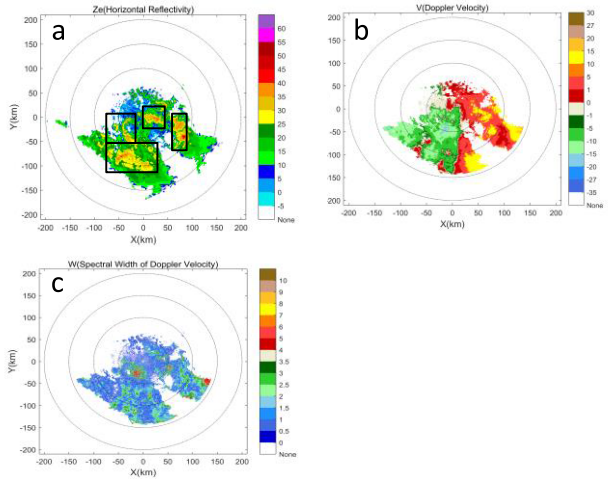

FIGURE 7. Real weather radar echo images corresponding to rainfall phenomena. Figure 7(a) is reflectivity image. Figure 7(b) is velocity image. Figure 7(c) is spectral width image.

TABLE 3. Parameters in neural network training.

Parameter	value
Image scale	[-1, 1]
Optimizer	Adam
Learning rate	2e-4
Momentum bate	0.5
Batch size	16
Training iterations number	40

B. THE SIMULATION RESULTS OF DCGAN

DCGAN's experimental hardware environment is: NVIDIA Tesla P40 GPU, CUDA 9.1, Ubuntu 16.04, memory 24GB. TensorFlow 1.4 and Python3.6 are used as the software. The training datasets used in the experiment are as shown above. Some parameters in neural network training are configured as shown in the following table.

When the DCGAN training is completed, the generator can generate data samples that have the same distribution with the real data. Figure 8 shows the simulated weather radar echo images (base data) corresponding to rainfall phenomena

Three kinds of rainfall phenomena weather radar echo images are selected for analysis in this paper. As shown in Figure 8(a), the reflectivity is characterized by high intensity and large areas. There are positive and negative velocity regions which are symmetric to the radar station approximately and the maximum radial wind speed is more than 12m/s in the velocity echo image. The distribution of the spectral width is basically around 2m/s.

Figure 8(b) is the generated squall line process. The regions where the reflectivity has a part of the intensity are distributed along the squall line. The squall line passes through the radar station, so there is a clear positive and negative speed zone. The distribution structure of the spectral width is also substantially identical to the reflectivity distribution.

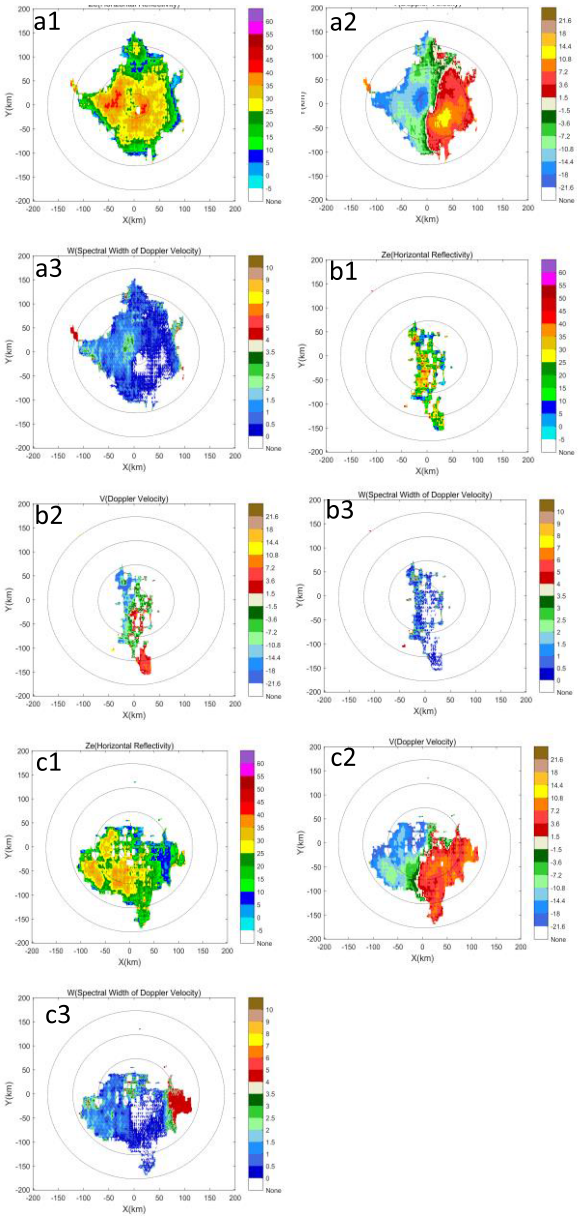

FIGURE 8. Simulated weather radar echo images corresponding to rainfall phenomena. Figure 8(a1), 8(b1), 8(c1) are reflectivity images. Figure 8(a2), 8(b2), 8(c2) are velocity images. Figure 8(a3), 8(b3), 8(c3) are spectral width images.

Figure 8(c) can be regarded as a rainfall process containing supercell. There are multiple strong reflectivity areas and the gradients in these areas are large, so these areas can be considered as areas where supercell may appear. Figure 8(c2) is a velocity image with significant positive and negative velocity regions in the radial direction. The distribution characteristics of the spectral width are basically consistent with that of the velocity.

These distribution characteristics are consistent with the general law of rainfall phenomena which is mentioned in Section 4.1. Besides, the cause of rainfall can be distinguished, such as squall line, supercell and so on.

In summary, the typical weather radar base data generated by the DCGAN have the distribution characteristics of real weather radar base data.

C. THE PERFORMANCE OF APS

Assuming a set of weather radar base data which are $Z = 25dBz$, $\delta_r = 3.5m/s$ and $v_r = 1, 2, \cdots 25$m/s. The data are used as the input of PS and APS respectively to simulate baseband I/Q time-domain sequences. Then the FFT transform algorithm is applied to the I/Q time-domain sequences to recover the weather radar base data. The comparison of the recovered and the originally assumed weather radar base data can be taken as a reference to verify the performance PS and APS. The comparison results are shown in Figure 9. REAL represents the originally assumed weather radar base data. The maximum errors of reflectivity, velocity and spectral width with APS are 1.41, 0.32 and 0.25, respectively. And the corresponding maximum errors with PS are 1.48, 3.32 and 1.35, respectively. It shows that the APS has more accuracy than PS in baseband weather radar echo signal generation.

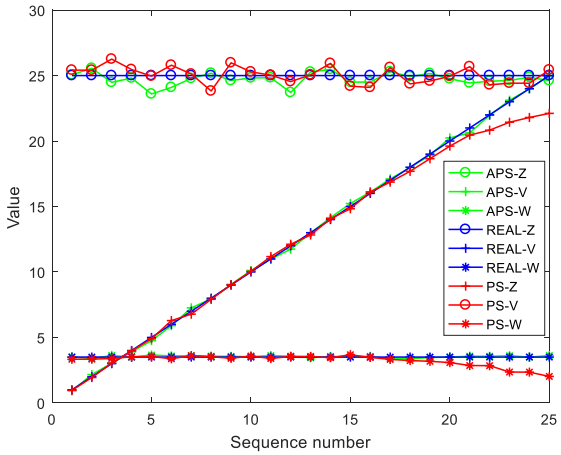

FIGURE 9. The comparison of originally assumed and recovered radar base data from the I/Q signals generated by APS and PS.

In this paper, the weather radar base data generated by DCGAN are applied as the input of APS to generate the baseband weather radar echo signals. Moreover, the baseband weather radar echo signals can be used in the test of radar signal processing unit. In order to verify the correctness of the baseband weather radar echo signals, they are converted into the radar base data by using FFT algorithm. By comparing Figure 10 and Figure 8(a), it can be seen that the distributions of the two radar base data are consistent. In addition, a quantitative error analysis method of weather radar base data is proposed by selecting valid data for calculation. The valid data are defined that the value of reflectivity, velocity and spectral width are in the valid range. The formula is as follows:

$$\rho = \sum_{i=1}^{N} \frac{(|A_i(valid) - B_i(valid)|)}{M} \tag{16}$$

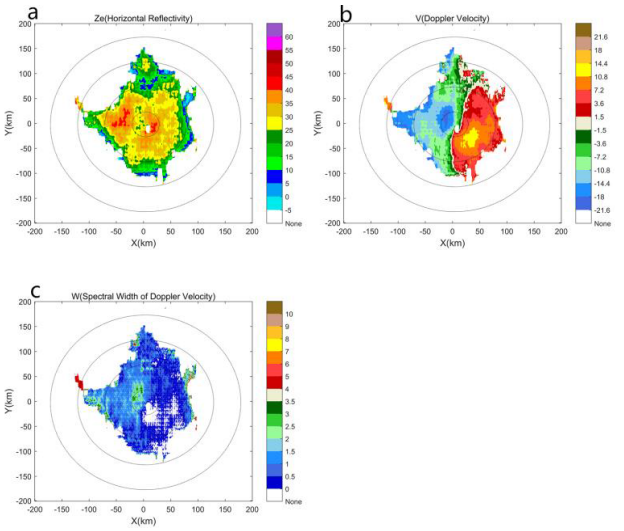

FIGURE 10. The recovered weather radar echo images. Figure 10(a) is reflectivity image, Figure 10(b) is velocity image, and Figure 10(c) is spectral width image.

Here, N is the number of the weather radar base data, M is the number of valid weather radar base data, A is the value of original weather radar base data and B is the value of simulated weather radar base data. The average errors of reflectivity, velocity and spectral width are 0.9422, 0.0738 and 0.0452 respectively. The maximum errors of reflectivity, velocity and spectral width are 4.123, 0.5522 and 0.3761. Though some reflectivity errors are big due to the small spectral width, most of the errors are in a reasonable range. In conclusion, APS performs better than PS and has practical value.

V. DISCUSSION

As mentioned above, the available typical weather radar data are difficult to meet the needs of current weather radar research. In recent years, a great number of studies have focused on the generation of the typical weather radar base data. These traditional methods have a common shortcoming that they can only generate a single radar product data without considering the correlation between multiple product data. There is a big deviation between the generated product data and the real data. In this paper, the DCGAN is applied to generate the typical weather radar base data, which is widely used in the generation of sample data because of the strong feature extraction and learning ability. In this method, the reflectivity, velocity and spectral width data are generated by using a noise sequence as input. Moreover, the relationships between multiple radar product data are fully considered, which make the generated weather radar base data closer to the real weather radar base data.

In order to convert the radar base data generated by DCGAN into the radar echo signals without distortion, a new power spectrum algorithm is proposed in this paper, which is referred to as APS. Compared with the traditional algorithm, the spectrum scope is adjusted according to the velocity adaptively in APS. The problem of power spectrum components loss caused by too large or too small of the velocity data is avoided, which makes the generated test signal closer to the real radar echo signal.

However, the training process of DCGAN usually requires large labeled data and powerful computational resources. It is obvious that the training samples described in Section II are insufficient. Future work should be focused on collecting more samples for training the DCGAN. Moreover, the generated data corresponding to the weather type are rainfall in this paper. More kinds of precipitation data are needed in the meteorological services, such as snow, hail, and so on. Future work should change the DCGAN to generate multiple types of radar base data.

VI. CONCLUSION

In this paper, the DCGAN network is applied to generate the weather radar base data. Experiment shows that the DCGAN can generate multiple radar product data simultaneously, including the reflectivity, velocity and spectral width data. Moreover, the relationships between multiple radar product data are fully considered in this method, which make the generated radar base data more similar with the real radar base data. In addition, a new power spectrum algorithm is proposed in this paper, which can adjust the spectrum scope according to the velocity adaptively. It is applied to a transformation which turns the radar base data into the baseband weather radar echo signals. The generated radar echo signals are more accurate than the calculation results of the traditional power spectrum algorithm.

REFERENCES

[1] L. Baldini, N. Roberto, M. Montopoli, and E. Adirosi, "Ground-based weather radar to investigate thunderstorms," in *Remote Sensing of Clouds and Precipitation*. Cham, Switzerland: Springer, 2018, pp. 113–135.
[2] D. S. Zrnić, "Simulation of weatherlike Doppler spectra and signals," *J. Appl. Meteorol.*, vol. 14, no. 4, pp. 619–620, Jan. 1975.
[3] D. S. Zrnić, "Estimation of spectral moments for weather echoes," *IEEE Trans. Geosci. Electron.*, vol. 17, no. 4, pp. 113–128, Apr. 1979.
[4] R. J. Doviak, D. S. Zrnic, and R. M. Schotland, "Weather signal processing," in *Doppler Radar and Weather Observations*. Millbrae, CA, USA: Academic, 1993, pp. 121–172.
[5] O. Bousquet and B. F. Smull, "Airflow and precipitation fields within deep alpine valleys observed by airborne Doppler radar," *J. Appl. Meteorol.*, vol. 42, no. 10, pp. 1497–1513, 2003.
[6] A. Lupidi, C. Moscardini, F. Berizzi, and M. Martorella, "Simulation of X-band polarimetric weather radar returns based on the weather research and forecast model," in *Proc. IEEE Radar Conf.*, May 2011, pp. 734–739.
[7] S. Lischi, A. Lupidi, M. Martorella, F. Cuccoli, L. Facheris, and L. Baldini, "Advanced polarimetric Doppler weather radar simulator," in *Proc. 15th Int. Radar Symp. (IRS)*, Jun. 2014, pp. 1–6.
[8] X. Zhengang, H. Xia, X. Liren, and Z. Zhengyu, "Model simulation of hazardous weather radar echo," *Chin. J. Stereol. Image Anal.*, vol. 20, no. 3, pp. 267–273, 2015.
[9] I. Goodfellow *et al.*, "Generative adversarial nets," in *Advances in Neural Information Processing Systems*. San Mateo, CA, USA: Morgan Kaufmann, 2014, pp. 2672–2680.
[10] O. Wenqi and X. Kun, "Mask-to-human: Conditional human image synthesis using generative adversarial networks," *China Sciencepaper*, vol. 14, no. 3, pp. 255–260, 2019.
[11] Z. Guanghua, W. Fubao, and D. Weijun, "Study on star-galaxy image generation method based on GAN," *J. Northwestern Polytech. Univ.*, vol. 37, no. 2, pp. 315–322, 2019.

[12] P. Isola, J.-Y. Zhu, T. Zhou, and A. A. Efros, "Image-to-image translation with conditional adversarial networks," 2016, *arXiv:1611.07004*. [Online]. Available: https://arxiv.org/abs/1611.07004
[13] C. Yuanzhao *et al.*, "A study on the artificial intelligence nowcasting based on generative adversarial networks," *Trans. Atmos. Sci.*, vol. 42, no. 2, pp. 311–320, 2019.
[14] A. Radford, L. Metz, and S. Chintala, "Unsupervised representation learning with deep convolutional generative adversarial networks," 2015, *arXiv:1511.06434*. [Online]. Available: https://arxiv.org/abs/1511.06434
[15] P. L. Suárez, A. D. Sappa, and B. X. Vintimilla, "Infrared image colorization based on a triplet DCGAN architecture," in *Proc. IEEE Conf. Comput. Vis. Pattern Recognit. Workshops*, Jul. 2017, pp. 212–217.
[16] Z. Chun, W. Hanli, W. Tianyuan, and W. Wei, "Speech generation based on depth convolution for adversarial networks," *Instrum. Technol.*, no. 2, pp. 13–15 and 20, 2018.
[17] Z. Peichang *et al.*, "Radar constant," in *Radar Meteorology*. Beijing, China: China Meteorological Press, 1988, pp. 88–89.
[18] A. Monakov and Y. Monakov, "Error analysis of pulse-pair estimates," *IEEE Trans. Aerosp. Electron. Syst.*, vol. 47, no. 3, pp. 2222–2230, Jul. 2011.
[19] J. Shen, L. Wang, and Z. Qin, "Doppler frequency and its changing rate estimation by pulse pair processing or FFT techniques," in *Proc. Int. Conf. Radar*, 1986, pp. 319–324.
[20] G. Xuepeng *et al.*, "A study on quantitative estimation of precipitation Z-I relationship by Bijie CINRAD/CD radar," *J. Technol. Wind*, no. 1, pp. 77–78, 2017.
[21] V. M. Melnikov and R. J. Doviak, "Spectrum widths from echo power differences reveal meteorological features," *J. Atmos. Ocean. Technol.*, vol. 19, no. 11, pp. 1793–1810, 2002.
[22] Z. Zhenqian *et al.*, "A study on weather radar precipitation echo signal characteristics," *Modern Radar*, vol. 38, no. 9, pp. 12–16, 2016.